Possibilities of Assembling of Processing Maps by Utilizing of an Artificial Neural Network Approach

P Opěla[1], I Schindler[1], S Rusz[1], P Kawulok[1], R Kawulok[1], V Ševčák[1]

[1] VSB – Technical University of Ostrava, Ostrava, Czech Republic, EU

E-mail: petr.opela@vsb.cz

Abstract. The processing maps (i.e. power dissipation maps superimposed over instability maps) can be used as a very convenient tool in case of an optimizing of hot forming processes. In this research, processing maps of C45 medium-carbon steel were assembled on the basis of an experimental flow stress dataset. This dataset was acquired via series of uniaxial hot compression tests in the temperature range of 1173 K – 1553 K and the strain rate range of 0.1 s^{-1} – 100 s^{-1}. In addition, a predicted flow stress dataset was created with use of an artificial neural network approach – it allowed extending of the experimental dataset with additional temperature levels. The experimentally compiled processing maps have been subsequently enhanced by this additional dataset to encourage the overall information capability. The results have showed that the predicted dataset was useful to reveal additional instability regions in the experimentally assembled processing maps.

1 Introduction

In recent years, it has been showed that so-called processing maps are a very useful tool for an optimizing of hot forming processes. These maps simply represent the areas of temperature, strain rate and strain which are appropriate to use in a forming process. They, of course, also denote the areas at which the forming process becomes to be precarious [1, 2]. The processing maps are compiled by superimposing of power dissipation maps over instability maps. These maps are usually assembled by means of experimental flow stress data which are acquired by e.g. uniaxial hot compression or torsion tests. These tests are performed at given combinations of temperatures and strain rates – covering a presumed range of concrete forming process. However, the limited amount of the experimental flow stress data can lead to an inferior accuracy of the assembled processing maps. Nevertheless, this issue can be overcome by utilizing of a predicted flow stress dataset [3]. Flow stress prediction is usually performed by so-called flow stress models. These models contain different parameters (auxiliary variables), e.g. peak point coordinates, hardening and softening exponents. These parameters are dependent on the thermomechanical conditions (i.e. temperature, strain rate), so they need to be related to these thermomechanical circumstances [4]. In this work, in the first place, power dissipation and instability maps of the C45 medium-carbon steel have been compiled on the basis of an experimental flow stress dataset. These maps were then enhanced by a predicted flow stress dataset (assembled with use of an artificial neural network approach). The aim of this research is to determine the influence of the additional flow stress dataset on completeness of the assembled processing maps.

2 Experimental flow stress dataset

Experimental flow stress dataset of the C45 medium-carbon steel was acquired by means of series of uniaxial hot compression tests. The entire experimental procedure was in detail described previously in [5]. The tests were performed at the deformation temperatures (T) of 1553 K, 1473 K, 1373 K, 1273 K, 1173 K and the strain rates ($\dot{\varepsilon}$) of 0.1 s^{-1}, 1 s^{-1}, 10 s^{-1}, 100 s^{-1}, upon the true strain (ε) up to 1.0. Afterward, twenty flow curves (i.e. dependence of true flow stress on true strain at given thermomechanical conditions) were assembled on the basis of this experimental dataset.

3 Predicted flow stress dataset

3.1 Hot flow stress models

The experimentally compiled flow curves were described via known flow stress models. Cingara and McQueen's model [6] was used to describe these curves in the strain range of $0 \leq \varepsilon \leq \varepsilon_p$ (i.e. up to the peak point) – see equation (1). A modified version of this model [7] was then applied to describe the curves in the strain range of $\varepsilon_p \leq \varepsilon$ (i.e. beyond the peak point) – see equation (2):

$$\sigma = \sigma_p \cdot \left[\frac{\varepsilon}{\varepsilon_p} \cdot \exp\left(1 - \frac{\varepsilon}{\varepsilon_p}\right)\right]^c \tag{1}$$

$$\sigma = \sigma_{ss} + \left(\sigma_p - \sigma_{ss}\right) \cdot \left[\frac{\varepsilon}{\varepsilon_p} \cdot \exp\left(1 - \frac{\varepsilon}{\varepsilon_p}\right)\right]^s \tag{2}$$

In the equations (1) and (2), ε (-) is true strain and σ (MPa) is corresponding flow stress. The subscript p indicates the coordinates of maximum flow stress level (so-called peak point) and subscript ss corresponds to the initiation of steady-state flow. The variables c (-) and s (-) represent the work-hardening exponent and softening exponent, respectively [6, 7].

3.2 Description of the flow stress models parameters via an artificial neural network approach

The flow stress models parameters (i.e. ε_p, σ_p, σ_{ss}, c and s) are highly dependent on the temperature and strain rate level – so they need to be related to these thermomechanical circumstances before use in the models (1) and (2) [6, 7].

As the very first step, the experimental values of these parameters have to be obtained. The values of ε_p, σ_p and σ_{ss}, can be easily deducted at each combination of temperature and strain rate from the experimentally compiled flow curves. The experimental values of work-hardening exponent, c, can be obtained via regression analysis of the logarithmic form of equation (1), i.e. $\ln(\sigma / \sigma_p)$ vs. $\ln(\varepsilon / \varepsilon_p) + 1 - \varepsilon / \varepsilon_p$. Similarly, it is possible to achieve the values of work-softening exponent, s, from the logarithmic form of equation (2), i.e. $\ln[(\sigma - \sigma_{ss}) / (\sigma_p - \sigma_{ss})]$ vs. $\ln(\varepsilon / \varepsilon_p) + 1 - \varepsilon / \varepsilon_p$ [6, 7].

As the second step, an artificial neural network approach was utilized to mathematically describe the obtained experimental values of the above mentioned parameters. A Multi-Layer Feed-Forward Artificial Neural Network (ANN) with the Back-Propagation (BP) learning algorithm is the most used type of ANN in case of the material modeling [3]. This type of ANN was used to create five neural networks – one network for each examined parameter. Architecture of the generated networks was relatively simple. Each network connects the input variables (temperature and strain rate) with the output variable (one of the examined parameters) via set of artificial neurons arranged in three layers, see figure 1.

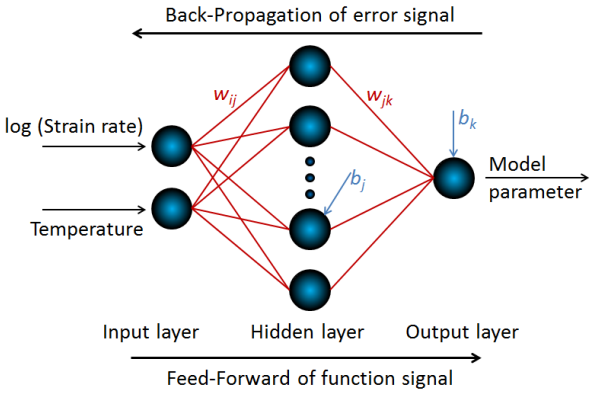

Figure 1. Schematic illustration of the used artificial neural network architecture.

The neurons inside of the neural network are connected via synaptic weights – w_{ij} (connecting input and hidden layer) and w_{jk} (connecting hidden and output layer). Each neuron of the hidden and output layer is at the same time connected with a unique bias value (b_j, b_k). This weights and biases must be then properly set to get the correct response of the network (provided by a network training process) [3]. Detailed specifications of the architecture of the created networks are presented in table 1. Appropriate number of neurons in the hidden layer of given network is clearly shown in table 2. Comparison of the experimental and predicted flow curves can be seen in figure 2.

Table 1. Architecture of the assembled artificial neural networks.

Network architecture parameter	**Settings**
Network type	Multi-Layer
Propagation of function signal	Feed-Forward
Learning (training) type	With supervisor
Learning (training) algorithm	Back-Propagation of error signal (BP)
Performance function	Mean Square Error (MSE)
Minimization algorithm of performance function	Levenberg-Marquardt (LM)
Hidden layer transfer function	Hyperbolic tangent sigmoid (tansig)
Output layer transfer function	Linear (purelin)

Table 2. Appropriate number of neurons in the hidden layer of given network.

Network intended for the parameter	ε_p	σ_p	σ_{ss}	c	s
Ideal hidden layer neuron number	5	3	3	8	6

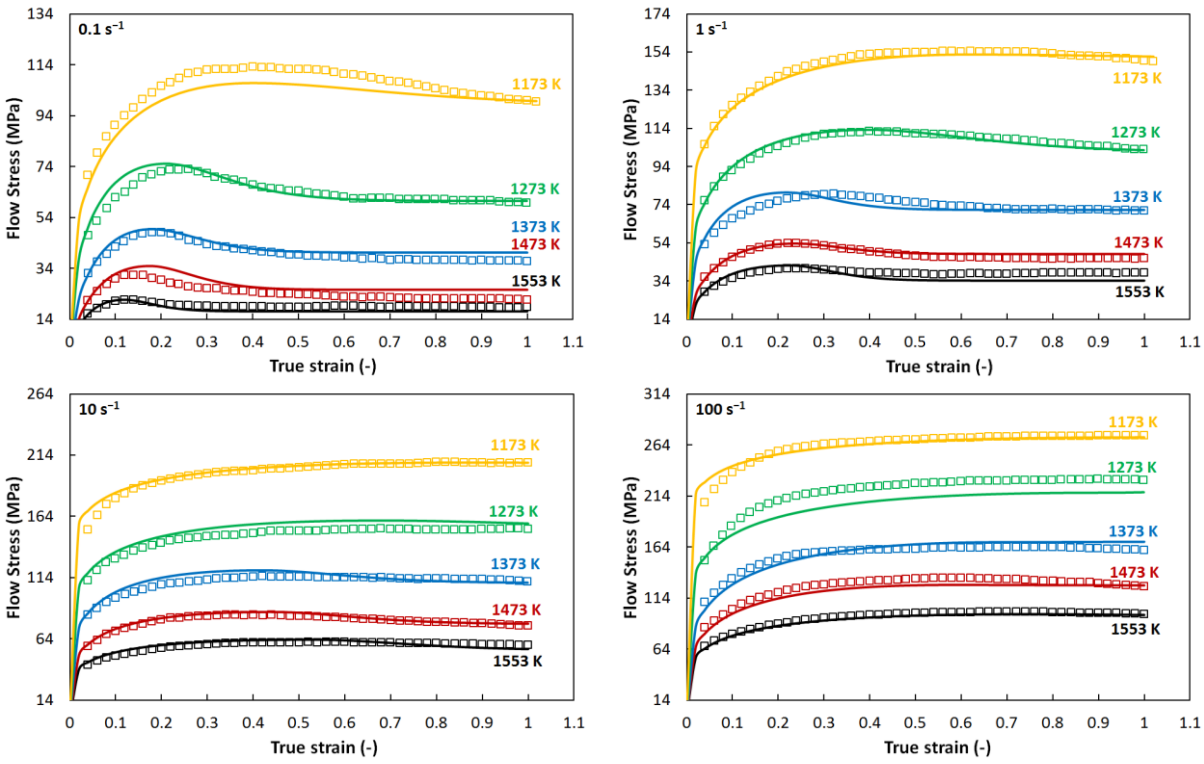

Figure 2. Experimental flow curves (squares) and predicted flow curves (lines) of the steel C45.

It can be seen, the flow tress level of the examined medium-carbon steel is highly dependent on temperature and strain rate – flow stress decreases significantly with an increase of temperature and

decrease of strain rate. The course of the flow stress is also highly influenced by a combination of the thermomechanical parameters – see e.g. observation of peak point or steady-state flow in dependence on temperature and strain rate level. It can be noted, the observed flow stress behavior was possible sufficiently described by means of the above mentioned models (1) and (2) in combination with the ANN approach.

4 Processing maps

In this investigation, processing maps of the examined medium-carbon steel were assembled on the basis of so-called Dynamic Material Model (DMM) [8 – 10]. According to the DMM, the material passing through thermoplastic deformation can be considered as a power dissipater [11]. The instantaneous power per unit volume, P (J), which is dissipated by the formed material consist of two complementary parts – G (J) and J (J). The first one is the power dissipated as a consequence of temperature increase with respect to plastic deformation. The second one is the power consumed by metallurgical processes, e.g. dynamic recovery (DRV) and recrystallization (DRX) or defect formation [1, 2, 12]. The power dissipation can be quantified on the basis of so-called efficiency of power dissipation, η (-) [8]:

$$\eta = \frac{2 \cdot m}{m+1} \tag{3}$$

In equation (3), m (-) is the strain rate sensitivity index which determines the correlation between the G content and J co-content – it can be expressed as [1]:

$$m = \frac{dJ}{dG} = \frac{\dot{\varepsilon} d\sigma}{\sigma d\dot{\varepsilon}} = \frac{d \ln \sigma}{d \ln \dot{\varepsilon}} \tag{4}$$

In equation (4), σ (MPa) is the instantaneous flow stress at given strain and temperature level, and $\dot{\varepsilon}$ (s^{-1}) is the strain rate [1] – the relevant data can be obtained from the flow stress dataset. It should be noted, the data points of ln σ vs. ln $\dot{\varepsilon}$ should be fitted by cubic spline [11]. A graphical representation of the efficiency of power dissipation with respect to temperature and strain rate is known as so-called power dissipation maps [1, 12]. These maps simply reveal various domains which correlate with specific microstructural processes (e.g. DRV, DRX) [11]. Each microstructural process is associated with the specific η-range, e.g. η-values in the range of 30 – 50 % are typical for the DRX process and η-values above of 60 % are then attributed to superplasticity [12]. In order to detect the regimes of flow instability during hot deformation, a continuum criterion was proposed by Kumar [13] and Prasad [14] on the basis of Ziegler's [15] principle of maximum rate of entropy production. In accordance with this criterion, flow instability can occur if [1]:

$$\xi(\dot{\varepsilon}) = \frac{\partial \ln\left(\frac{m}{m+1}\right)}{\partial \ln \dot{\varepsilon}} + m \leq 0 \tag{5}$$

In equation (5), $\xi(\dot{\varepsilon})$ is the parameter of flow instability. The variation of this parameter with temperature and strain rate is then known as flow instability map [1]. The above mentioned processing maps are then given by superimposing of the flow instability maps over the power dissipation maps [11].

With use of the above described approach, the processing maps of the medium-carbon steel C45 were assembled on the basis of two flow stress datasets. The first one is given by the experimental procedure. So, the experimental processing maps were compiled with use of five temperatures (1553 K, 1473 K, 1373 K, 1273 K and 1173 K) and four strain rates (0.1 s^{-1}, 1 s^{-1}, 10 s^{-1}, 100 s^{-1}). The second one is obtained on the basis of the mathematical description of the experimental dataset – when the flow stress was predicted at additional temperature levels. So, the predicted processing maps were compiled with use of ten temperatures (1553 K, 1523 K, 1473 K, 1423 K, 1373 K, 1323 K, 1273 K, 1223 K, 1173 K and 1073 K) and four strain rates (0.1 s^{-1}, 1 s^{-1}, 10 s^{-1}, 100 s^{-1}). The processing maps were compiled at true strains of 0.2, 0.4, 0.6 and 0.8. Figure 3 shows the processing maps created altogether on the basis of experimental and predicted flow stress data. The contours clearly show the

efficiency of power dissipation, η, in percent. As mentioned above, the η-values in the range of 30 – 50 % are typical in case of DRX process [12]. Based on this assumption, it can be concluded, the examined steel is undergoing through the DRX which is, of course, gradually evolved by an increasing strain level.

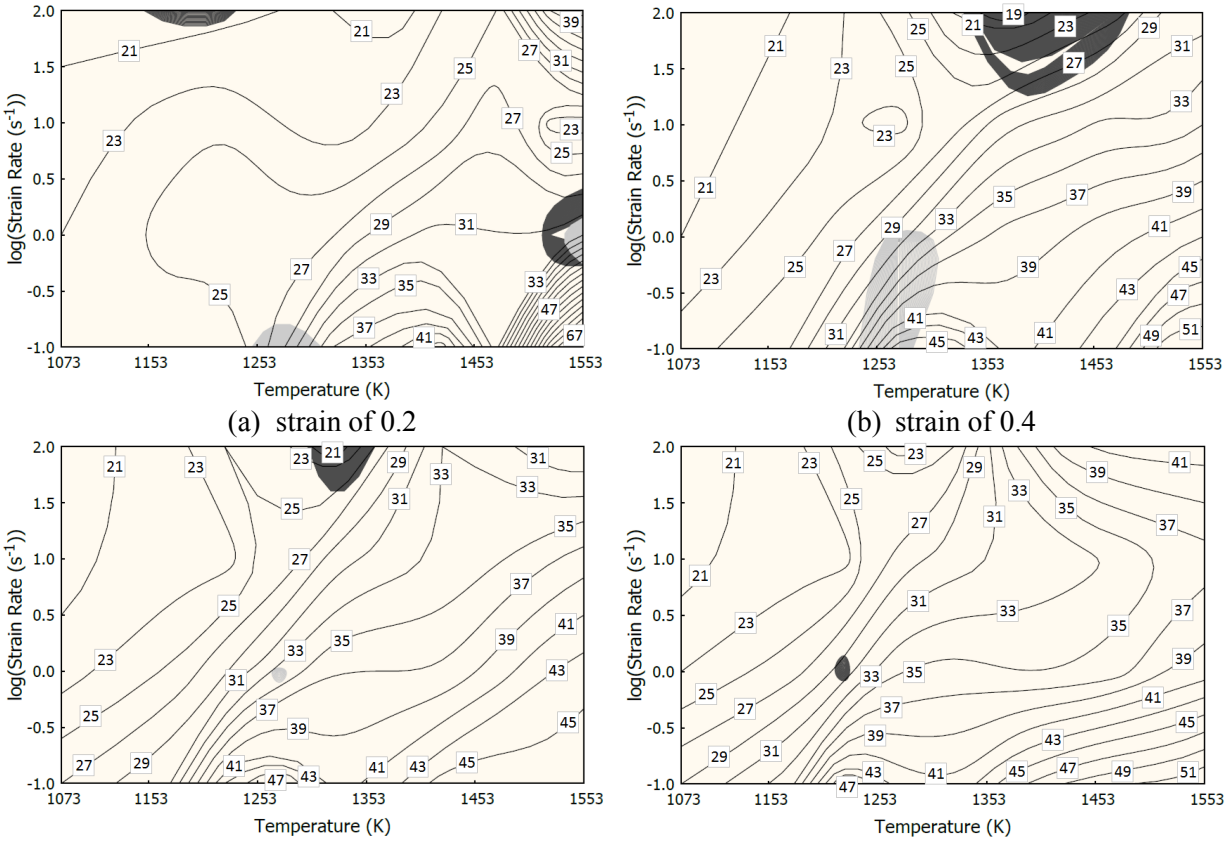

Figure 3. Processing maps of the steel C45; experimental instability (light gray areas) and predicted instability (dark grey areas).

It should be noted, the high value of power dissipation efficiency does not mean the necessarily unproblematic forming conditions. So, the flow instability criterion should be taken into account. The shaded areas represent the flow instability domains. Note there are two types of instability domains. The first one (light gray areas) corresponds to the instability domains which were revealed on the basis of the experimental flow stress dataset. The second one (dark grey areas) then relates to the instability domains which were achieved on the basis of the predicted flow stress dataset. It can be seen, there are two experimentally revealed instability domains at strain of 0.2. The first one is nearby the temperature of 1253 K and around the strain rate of 0.1 s^{-1}. The second one is around of 1553 K and 1 s^{-1}. This second domain is, however, somewhat extended by the predicted flow stress dataset. In addition, the predicted dataset revealed another instability domain near to the temperature of 1153 K and strain rate of 100 s^{-1}. Two distinct areas of instability flow are clearly visible at the strain of 0.4. The first one was calculated on the basis of the experimental dataset in the vicinity of 1253 K and the strain rate range of 0.1 s^{-1} – 1 s^{-1}. The second one was revealed on the basis of predicted dataset in the temperature range of 1353 K – ca 1500 K and strain rate range of ca 17 s^{-1} – 100 s^{-1}. Quite different situation occurs at the strain of 0.6. The experimental flow stress dataset reveals very insignificant instability area (close to 1253 K and 1 s^{-1}). Nevertheless, the predicted dataset allowed revealing of instability area at the temperature range of 1300 K – 1353 K and the strain rate range of 32 s^{-1} –

100 s^{-1}. Only one tiny instability area can be then observed at the strain of 0.8 – revealed just on the basis of the predicted dataset. Based on the above performed analysis can be stated, the experimental flow stress dataset can be insufficient in case of revealing of instability flow areas. The additional (predicted) flow stress dataset can be then used to reveal other areas of instability flow, so the assembled processing maps could be hypothetically more accurate. This hypothesis, however, should be proved by metallographic analyses.

5 Conclusion

Experimental flow curves of the C45 medium-carbon steel were mathematically described by means of two flow stress models in combination with an artificial neural network approach. Additional flow curves were then predicted to extend the experimental dataset. The experimental and predicted datasets were then used to compile processing maps of the examined steel. Results have showed the additional (predicted) dataset is helpful to reveal higher amount of flow instability areas. This fact should lead to the greater information capability of the assembled processing maps. Nevertheless, the metallographic analyses should be performed to confirm this assumption.

Acknowledgements

This paper was created on the Faculty of Metallurgy and Materials Engineering in the Project No. LO1203 "Regional Materials Science and Technology Centre – Feasibility Program" funded by Ministry of Education, Youth and Sports of the Czech Republic.

References

[1] Gao X, Jiang Z, Wei D, Jiao S and Chen D 2014 *Key Eng. Mater.* **622-623** 330–39
[2] Kliber J 2016 *Materials Physics and Mechanics* **25** 16–21
[3] Quan G-Z, Zou Z-Y, Wang T, Liu B and Li J-Ch 2017 *High Temp. Mater. Processes* **36** 1–13
[4] Gronostajski Z 2000 *J. Mater. Process. Technol.* **106** 40–44
[5] Opěla P, Schindler I, Kawulok P, Vančura F, Kawulok R, Rusz S and Petrek T 2015 *Metalurgija* **54** 469–72
[6] Cingara A and McQueen H J 1992 *J. Mater. Process. Technol.* **36** 31–42
[7] Opěla P, Schindler I, Kawulok P, Vančura F, Kawulok R and Rusz S 2016 Proc. 25th Anniversary International Conference on Metallurgy and Materials (Brno) (Ostrava: Tanger Ltd) p 458
[8] Prasad Y V R K, Gegel H L, Doraivelu S M, Malas J C, Morgan J T, Lark K A and Barker D R 1984 *Metall. Trans.* A **15** 1883–92
[9] Gegel H L, Malas J C, Doraivelu S M and Shende V A 1987 Metals Handbook vol 14, (ASM International) p 417
[10] Alexander J M 1989 Modelling Hot Deformation of Steels, ed J G Lenard (Berlin: Springer-Verlag) p 101
[11] Quan G-Z, Zhao L, Chen T, Wang Y, Mao, Y-P, Lv W-Q and Zhou J 2012 *Mater. Sci. Eng.* A **538** 364–73
[12] Sonnek P and Petruželka J 2001 Proc. 10th International Metallurgical and Materials Conference (Ostrava) (Ostrava: Tanger Ltd)
[13] Kumar A K S K 1987 Master's Thesis (Bangalore: Indian Institute of Science)
[14] Prasad Y V R K 1990 *Indian J. Technol.* **28** 435–51
[15] Ziegler H 1963 Progress in Solid Mechanics vol 4, (New York: John Wiley and Sons) p 93